Fermi National Accelerator Laboratory

FERMILAB-Pub-90/041-E

[E-632]

A System for Viewing Holograms*

R. Naon, H. Bjelkhagen, R. Burnstein, and L. Voyvodic
Fermi National Accelerator Laboratory
P.O. Box 500
Batavia, Illinois 60510

February 1990

* Published in Nucl. Instrum Methods A.

A SYSTEM FOR VIEWING HOLOGRAMS

R. NAON, H. BJELKHAGEN, R. BURNSTEIN and L. VOYVODIC

Fermilab, Batavia, IL 60510, USA

A holographic virtual image reconstruction machine was built for the replay of holograms taken in the Fermilab 15 ft Bubble Chamber. We discuss the major components of the holographic replay machine and the relevant construction details. Replay wavelengths different from the original recording wavelength are possible and corrected for in the system described. The resolution of the system is improved by using a liquid film gate. The usefulness of the system is enhanced by the flexibility of using a fiber optic reconstruction reference beam. A procedure for locating 15 ft Bubble Chamber events on the hologram is outlined.

1. Introduction

A modified in-line holographic system has been installed in the 15 ft Bubble Chamber detector at the Fermi National Accelerator Laboratory [1], in addition to a conventional photographic system. The holographic system was tested in the first run of the E-632 * experiment and was used during the second physics run of the experiment. The latter run produced 218 000 holograms of which 110 000 are useful for physics analysis. The holograms are recorded on 70 mm Agfa–Gevaert, Holotest 10E75 film and contain bubble images from a volume of the Bubble Chamber of approximately two cubic meters. The bubble images represent tracks of charged particles produced from high energy neutrino interactions. One of the main purposes of the experiment is to observe short lived particles. Our holographic system makes it possible to record smaller bubble images (≈ 100 μm) than possible with conventional photographs (≈ 500 μm) which record the entire visible chamber volume (28 m^3). This is due to the fact that conventional photography has limitations caused by diffraction of the camera lens aperture. About 20–30% of all interactions in the Bubble Chamber fall within the holographic volume. Consequently one aspect of the experiment is the inspection of a large number of holograms. For this reason, we have constructed a system for the reconstruction of holograms at Fermilab [2].

* E-632 is a collaboration of the following institutions: University of California Berkeley (USA), University of Birmingham (UK), IIHE Brussels (Belgium), CERN (Switzerland), Chandigarh-Panjab University (India), Fermilab (USA), University of Hawaii (USA), Imperial College London (UK), Illinois Inst. of Technology (USA), University of Jammu (India), Max-Plank Institute for Physics Munich (FRG), Oxford University (UK), Rutgers University (USA), Rutherford Appleton Laboratory (UK), DPhPE Saclay (France), Stevens Inst. of Technology (USA), Tufts University (USA). A detailed description of the holographic apparatus will be contained in a forthcoming paper to be submitted to Nucl. Instr. and Meth.

2. Design goals

The total sample of useful holograms is 110 000, contained on 70 mm film frames in 600 ft rolls. The task of looking at this large amount of film is formidable but has been simplified as follows. For every holographic frame of film there is a corresponding triad of conventional photographs of the Bubble Chamber taken on 70 mm Kodak 2482 RAR film. The projected images of the film are scanned by trained personnel who locate, categorize and measure the events. Once the vertex of an event is measured its position is known to a few millimeters in space. This information is then used to locate the vertex of the event on the hologram. This procedure is described in greater detail in section 5.2. The important consequence is that the sample of holograms that needs to be inspected is reduced from 110 000 to about 11 000, since only one of every three expansions contains an event and of those 20–30% are in the holographic volume. This is still a time consuming task and we have designed a system whose principal features are low cost, ease of operation and high resolution. The system described below exhibits these criteria.

3. General layout

The Fermilab reconstruction machine uses the virtual image for inspection of the holograms. In fig. 1 two

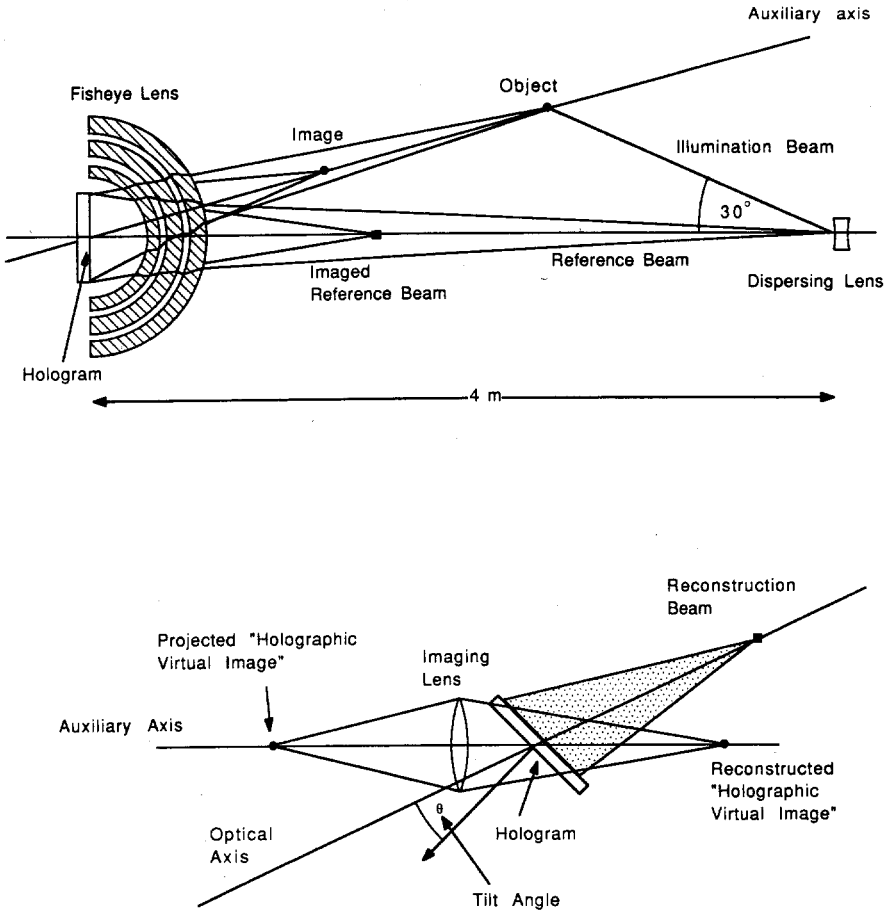

Fig. 1. Diagrams showing optical layouts. (Top) The recording layout. (Bottom) The virtual image reconstruction layout.

diagrams are displayed, showing the optical layout for recording and virtual image reconstruction. The entire system is comfortably contained in a room whose size is 2.5 m × 5.2 m. Fig. 2 shows a drawing of the general layout and fig. 3 is a photograph of the reconstruction machine. The principal features of the system are described in the following sections.

4. Technical considerations and construction details

4.1. Lasers

A JK ruby laser system 2000 with several modifications for pulse stretching [3,4] was used in producing the holograms made in the 15 ft Bubble Chamber. Two kinds of lasers were used in the Fermilab reconstruction scheme: a Lexel argon pumped dye laser using LDS 698 as the dye, and a 50 mW Spectra Physics He–Ne laser. The dye laser was used because of its ability to reproduce the ruby wavelength (694.3 nm) while the He–Ne laser was used because of its overall reliability and simplicity. The dye laser has drawbacks which contribute to its unreliable output performance, these include poor long and short term stability, and the necessity of a daily maintenance schedule. In addition to this the human eye, video camera, and film, all of which are utilized in reconstruction are more sensitive to the He–Ne wavelength. For these reasons, the He–Ne laser proved more useful. Short and long term stability of the laser are important properties in practice. For example, since focusing the holographic image is done by eye, it can be quite annoying if laser output is fluctuating at a rate less than 30 Hz. Maintenance of the dye laser involves time consuming operations which lead to long periods of down-time. Maintenance for our dye laser system includes: maintenance of argon laser cooling water, adjustment of the argon laser cavity mirrors, bi-monthly realignment of dye laser cavity mirrors, daily alignment of output fiber coupler, and periodic dye and

dye filter changes. This is in contrast to the He–Ne laser which requires no maintenance. Although different brands of dye lasers have varying reliability, the overall convenience that a He–Ne laser offers is obvious. The availability of a turn-key system during the production mode of operation makes the choice of a He–Ne laser compelling, assuming that the difference in wavelength does not affect the results. In fact we shall show in the section on resolution that for our system the image resolution obtainable for He–Ne is comparable to the results for the ruby wavelength. Therefore, in our case using the ruby wavelength would not significantly improve the image resolution.

4.2. Fiber optic reference illumination beam

A 6 μm single-mode step index optical fiber * is used as a flexible lightguide for illumination of the hologram as shown in fig. 4. The fiber takes the place of three optical components: the optical transport, a dispersing lens, and a spatial filter. The flexibility of the fiber has made it possible to have the laser separated from the reconstruction device. The less-used dye laser can also be merged into the optical path by means of another optical fiber and can be used at any time with little effort. The fisheye lens in the 15 ft Bubble Chamber is part of the holographic recording optics, and it is actually recorded in the hologram. Upon reconstruction of the hologram the transmitted reference beam is replaced by the single mode fiber (fig. 4). The numerical aperture of the fiber matches that of the original reference beam transmitted through the fisheye lens. In addition to this, the fiber acts like a spatial filter producing a beam with a good Gaussian profile.

4.3. Moving stage

The moving stage on which the holographic film platen is mounted is made up of two rotating stages: one mounted horizontally and the other vertically so that the axes are perpendicular and cross at a point in space. The moving stage allows the hologram and fiber to be rotated simultaneously on a rigid base providing azimuth and dip angles for viewing holographic images (fig. 4).

The rotating stages are manually driven, heavy machine tool tables: this type of stage was chosen for the following reasons. The rigidity of the hologram and reference beam base is important. The hologram and fiber need to be rigidly connected since the images viewed in holographic space are of the order of 10 μm and oscillations of 1 μm have been noticed which degrade the image quality. Although many optical quality stages provide sufficient mass, they are often very expensive and require motors and control electronics. In our system accurate positioning of the stages is not needed since no precision measurements are made using the stage. For this reason the inherent backlash and the other inaccuracies of an inexpensive machine tool table are of no consequence.

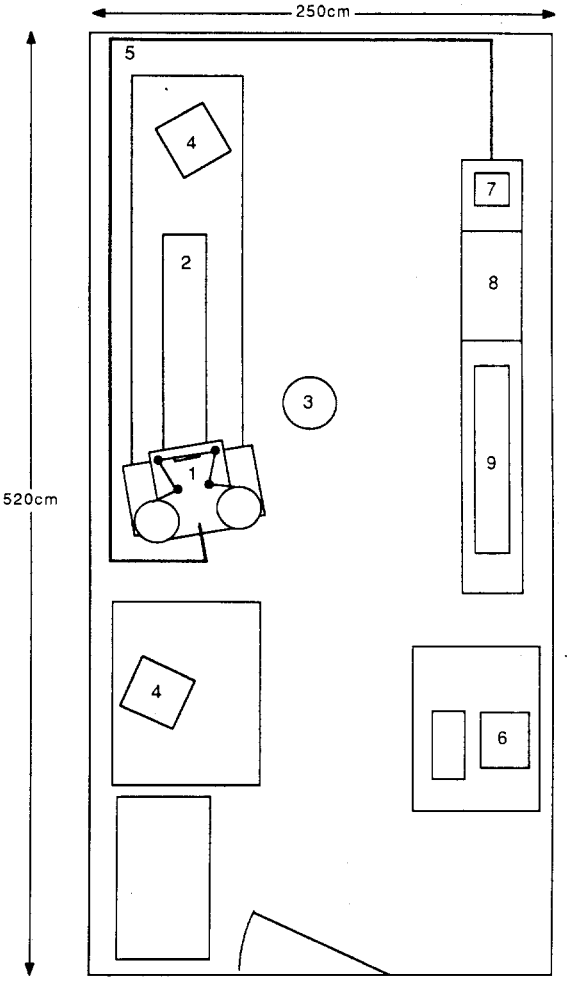

Fig. 2. General layout of reconstruction room. (1) Reconstruction machine; (2) optical focusing slide; (3) operators chair; (4) video monitors; (5) fiber optic conduit; (6) computer terminal; (7) fiber optic coupler; (8) dye laser; (9) argon pump laser.

4.4. Liquid film gate

The accurate positioning of the hologram with respect to the reconstruction wavefront is very important for the high resolution playback of holographic images. The ideal situation for reconstruction of the holographic image is to use a beam identical to the recording reference beam, that is one having the same wavelength, the same numerical aperture and the same position with

* Diaguide no. SS6-SY.

Fig. 3. Photograph of the Fermilab Holographic Virtual Image Reconstruction machine.

respect to the hologram. This is difficult to achieve but can be done in effect by making fine adjustments to the hologram orientation. These fine adjustments are made

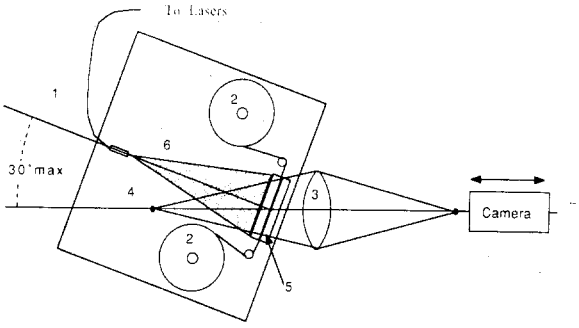

Fig. 4. Schematic layout of Virtual Image Reconstruction Machine. (1) Single-mode optical fiber; (2) film reels; (3) imaging lens; (4) holographic virtual image; (5) hologram and liquid film gate; (6) illumination laser light.

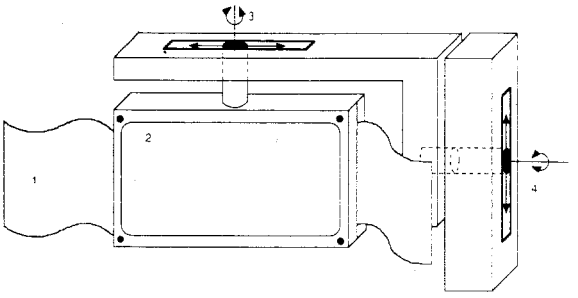

Fig. 5. Liquid film gate with four degrees of freedom. (1) Holographic film; (2) liquid film gate; (3) horizontal (x-axis) translational and rotation; (4) vertical (y-axis) translation and rotation.

by using a film platen which allows the holographic film four degrees of freedom; two tilts * and two translations. Fig. 5 shows the four degrees of freedom, x-axis translation and tilt and y-axis translation and tilt.

During the reconstruction process micro-positioning involves the translation and rotation of the hologram in small increments by the film stage with the four degrees of freedom provided. Micro-positioning of the hologram is needed to position the hologram in the correct location with respect to the illumination beam. It is essential for reducing the aberration of the holographic images. The procedure for fine tuning the image is straightforward and can be mastered within a few hours. Once the hologram is secured by the liquid film gate and the unfocused image located on the monitor (this is done simply by dialing up a position and focusing the camera), adjustments are made to each degree of freedom provided by the film stage while at the same time refocusing the video camera. The rotational degrees of freedom about the holographic axes x and y in fig. 5 are the primary adjustments and depend upon image angle. The translational adjustment in x and y does not change much from hologram to hologram.

The film platen also includes a liquid film gate. The liquid film gate itself consists of a device which sandwiches the hologram between two pieces of glass and allows an index matching liquid to be coated on both sides of the film [5]. A liquid used with good results is Decaline (decahydronaphalene) **. The film platen and liquid film gate combination performs three functions. The first is to clamp the film rigidly in place while the micro-positioning adjustments are made. Clamping the film with vacuum was tried but gave unsatisfactory results since dust trapped between the film and the glass

* Tilting of the hologram is actually a rotation of the hologram by small amounts about the two perpendicular axes which intersect at the center, in the plane of the hologram.

** Liquid film gates have been used extensively in the motion picture industry for film copying.

platen tends to deform the surface of the film; thus degrading the image quality. The second use of the liquid film gate, is to limit the amount of scattered light due to the scratches on the film. By using a liquid with an index of refraction close to that of the emulsion, the scratches are optically eliminated, which reduces the diffraction pattern produced by the scattered coherent light. Thirdly, the liquid film gate fills in depressions and imperfections on the surface of the film so that the surface of the film approaches optical flatness; thereby improving the overall image quality.

4.5. Imaging optics

A system of lenses is used for viewing the holographic virtual images. The lens system is positioned so that its optical axis intersects the hologram at its center, which is also the origin of the azimuth and dip angle positioning system. The lens system has a useful working distance of 25 cm $\pm$ 5 cm with a full numerical aperture of 0.16 at low magnification and 0.03 at high magnification. The fisheye optics used in the holographic camera demagnifies the image space by about a factor of ten so that resolution of the lens system at high magnification must be at least 10 μm to resolve bubbles of 100 μm in real space. We have tested the lens system with a bar test target and it achieves better than 10 μm resolution. In addition to this, the aperture of the front lens should equal that of the hologram since the resolution of the hologram is limited by its aperture; using a small aperture would limit the resolution and increase speckle noise. The optical system is made of a Nikkor 135 mm $f/2$ camera lens, a 50 mm Schneider $f/5.6$ enlarging lens and an image plane photosensitive device. A variety of magnifications of the image are achieved by manually moving the 50 mm lens and the image plane device on an optical rail, thereby simulating a zoom lens.

4.6. Camera and Vidicon

There are two types of image plane photosensitive devices incorporated in the reconstruction machine. The first device is a high resolution video system utilizing a Newvicon * tube with excellent sensitivity in the red and 800-line resolution. The video display is used to inspect and position the holograms. Certain of these holograms will require more detailed examination and to this end the virtual image is photographed using a 35 mm camera with a high magnification view finder. The film employed is Kodak Technical Pan (Kodak 2415), which has high contrast, high resolution and extended red sensitivity. Further analysis may be done by digitizing these projected negatives and using this data together with measurements of the conventional optical images of the same events.

* Hybrid Vidicon tube S4076 made by Matsushita Electronics Corp., Osaka, Japan.

5. Performance

5.1. Resolution of system

The next three sections discuss the sources and effects of image degradation during playback. No attempt is made to account for degrading effects which existed during the recording process and seem to distort the reference beam.

5.1.1. Aberrations and noise

There are two sources of aberration in this holographic system which can degrade the image: those due to the holographic process, and those due to geometrical aberrations that the fisheye lenses introduce.

The main source of holographic aberrations during reconstruction are due to the fact that the reconstruction reference beam differs from the recording reference beam in wavefront and wavelength. It is well known [6] that the two beams must be identical for aberration-free playback. Meier [7] and Champagne and Massey [8] have described holographic aberrations thoroughly, showing that five third-order aberrations (spherical aberration, coma, astigmatism, distortion, and field curvature) exist in holograms and can be described in terms of the following holographic parameters.

x_0, y_0, z_0	object position;
x_i, y_i, z_i	image position;
x_r, y_r, z_r, λ_r	recording beam position and wavelength;
x_c, y_c, z_c, λ_c	reconstruction beam position and wavelength;
m	magnification of the recorded interference pattern.

The aberrations that need be considered in our case are spherical aberration, coma, and astigmatism. These aberrations smear the bubble images destroying the point-to-point resolution described by the Rayleigh limit. Point-to-point resolution is important since the short-lived charm particles have mean decay lengths which are less than 200 μm. Of the three aberrations coma is the worst. Coma has a distinct tail associated with it and an asymmetric spot size; making the determination of the bubble image center difficult. Distortion and field curvature are less important since the field of view is small and the distortion of the image in our case is of little consequence. Other sources of holographic aberration are due to film limitations such as shrinkage and imperfections [9], and reference and reconstruction beam source size. When holograms are reconstructed using a liquid film gate these effects are small and will not be considered.

The aberrations created by the fisheye lens can be calculated by tracing rays through the lens and applying the methods used in common optical lens design. Combining this with the holographic resolution limit yields the ultimate limit on resolution for the system.

5.1.2. Effect of aberrations on resolution

The departure of the holographic image forming wavefront from the Gaussian reference sphere can be described in terms of the aberration coefficients S, C, A, representing spherical aberration, coma, and astigmatism respectively and the holographic parameter ρ which is the radius or half-aperture of the hologram [10]. Since the holograms are of the modified in-line type and symmetric about the center the geometrical aberration of the wavefront can be written as

$$\Delta = -\tfrac{1}{8}\rho^4 S + \tfrac{1}{2}\rho^3 C - \tfrac{1}{2}\rho^2 A, \tag{1}$$

neglecting field curvature and distortion. The geometrical aberration Δ is related to the change in phase $\Delta'\phi$ between the Gaussian reference sphere and image forming wavefront by $\Delta'\phi = (2\pi/\lambda_c)\Delta$. The coefficients C and A are functions of both x and y but because of the symmetry only one axis need be considered. The coefficients in terms of the holographic parameters for the virtual primary image are [11]

$$S = \frac{\mu}{m^4}\left[\left(1-\frac{\mu^2}{m^2}\right)\left(\frac{1}{z_o^3}-\frac{1}{z_r^3}\right) - \frac{3\mu}{z_c}\left(\frac{1}{z_o^2}+\frac{1}{z_r^2}\right) - 3\left(\frac{m^2}{z_c^2}-\frac{\mu^2}{m^2 z_o z_r}\right)\left(\frac{1}{z_o}-\frac{1}{z_r}\right) + \frac{6\mu}{z_o z_r z_c}\right], \tag{2}$$

$$C_x = \frac{\mu}{m z_c^2}\left(\frac{x_r}{z_r}-\frac{x_o}{z_o}\right) - \frac{\mu}{m^3 z_o^2}\left[\frac{x_o}{z_o}\left(\frac{\mu^2}{m^2}-1\right) + \frac{\mu x_c}{m z_c} - \frac{\mu^2 x_r}{m^2 z_r}\right] + \frac{\mu}{m^3 z_r^2}\left[\frac{x_r}{z_r}\left(\frac{\mu^2}{m^2}-1\right) - \frac{\mu x_c}{m z_c} - \frac{\mu^2 x_o}{m^2 z_o}\right] + \frac{2\mu}{m^2}\left(\frac{x_c}{z_c}+\frac{\mu x_o}{m z_o}-\frac{\mu x_r}{m z_r}\right) \times \left(\frac{1}{z_c z_r}-\frac{1}{z_o z_c}+\frac{\mu}{m^2}\frac{1}{z_o z_r}\right), \tag{3}$$

$$A_x = \frac{\mu x_c^2}{m^2 z_c^2}\left(\frac{1}{z_r}-\frac{1}{z_o}\right) - \frac{\mu x_o^2}{m^2 z_o^2}\left[\frac{1}{z_o}\left(\frac{\mu^2}{m^2}-1\right) + \frac{\mu}{z_c} - \frac{\mu^2}{m^2 z_r}\right] + \frac{\mu x_r^2}{m^2 z_r^2}\left[\frac{1}{z_r}\left(1-\frac{\mu}{m^2}\right) - \frac{\mu}{z_c} - \frac{\mu^2}{m^2 z_o}\right] + \frac{2\mu}{m}\left(\frac{1}{z_c}+\frac{\mu}{m^2 z_o}-\frac{\mu}{m^2 z_r}\right) \times \left(\frac{x_c x_r}{z_c z_r}-\frac{x_o x_c}{z_o z_c}+\frac{\mu x_o x_r}{m z_o z_r}\right), \tag{4}$$

where $\mu = \lambda_c/\lambda_r$. The magnification of the recorded interference pattern m is negligible hence $m = 1$. In the modified in-line holographic scheme the reconstruction beams are collinear with the z-axis, then $x_r = x_c = 0$. For the reconstruction and recording reference beams at the same distance along the z-axis, $z_r = z_c$ is true. We can also write $x_o/z_o = \sin\alpha_o$ in terms of object angle. The coefficients become:

$$S = \frac{\mu}{z_r^3 z_o^3}\left[z_o^3(\mu-2)(\mu-1) - z_r^3(\mu^2-1) + 3z_r z_o^2(\mu-1)\right], \tag{5}$$

$$C_x = \frac{\mu \sin\alpha_o}{z_r^2 z_o^2}\left[z_r^2(1-\mu^2) - z_o^2(1-\mu)^2 + 2\mu z_o z_r(\mu-1)\right], \tag{6}$$

$$A_x = \frac{\mu \sin^2\alpha_o}{z_o z_r}\left[z_r(1-\mu^2) + z_o(\mu^2-\mu)\right]. \tag{7}$$

Using the following values we can determine the coefficients S, C and A. The ratio of reconstruction wavelength to recording wavelength is

$$\mu = \frac{632.8\ \text{nm}}{694.3\ \text{nm}} = 0.9114,$$

the position of reference beam imaged through the fisheye lens is $z_r = 32$ cm and the center of the 15 ft Bubble Chamber imaged through the fisheye lens is $z_0 = 28$ cm. The coefficients are then

$$S = 1.269\times10^{-9}\ \text{mm}^{-3}, \tag{8}$$

$$C_x(\alpha_o) = 2.571\times10^{-7}\sin(\alpha_o)\ \text{mm}^{-2}, \tag{9}$$

$$A_x(\alpha_o) = 3.225\times10^{-4}\sin^2(\alpha_o)\ \text{mm}^{-1}. \tag{10}$$

To determine the limit of resolution in the presence of aberration a method of effective aperture is used. Using the wave front tolerance conditions for primary aberration given by Born and Wolf [12] and reproduced here in table 1, we can calculate the effective aperture. From eqs. (1) the departure from a perfect wavefront for spherical aberration only ($S \neq 0$) is as expressed in wavelengths

$$\left|\frac{X_{max}^4 S}{8\lambda}\right|, \tag{11}$$

for coma only ($C \neq 0$)

$$\left|\frac{X_{max}^3 C_x}{2\lambda}\right|, \tag{12}$$

Table 1
Tolerances for A_2C and S

Type of aberration	Tolerance condition [a]
Spherical aberration	≤ 0.94
Coma	≤ 0.60
Astigmatism	≤ 0.35

[a] For the case where the encircled energy is greater than 80%.

and for astigmatism only ($A \neq 0$)

$$\left| \frac{X_{\max}^2 A_x}{2\lambda} \right|, \tag{13}$$

where $X_{\max}$ is the effective radius of aperture for each aberration individually. Using the reconstruction wavelength $\lambda_c = 632.8$ nm and table 1 along with the expressions (11) we get an effective aperture $X_{\max}$ for spherical aberration of 43.9 mm. In the same way the effective aperture $X_{\max}$ for coma is

$$X_{\max} = \frac{14.342}{\sqrt[3]{\sin \alpha_o}}, \tag{14}$$

and for astigmatism

$$X_{\max} = \frac{1.171}{\sin \alpha_o}, \tag{15}$$

both given as functions of object angle α_o. Using these values of effective aperture and the resolution limit for a coherent imaging system [13],

$$\delta = \frac{0.82\lambda}{n \sin \theta}, \tag{16}$$

we can calculate the resolution limit for our holograms with aberrations. The numerical aperture $n \sin \theta$ can be replaced with $X_{\max}/Z$ for small numerical apertures, where Z is the object distance from the hologram in Bubble Chamber space. Then the resolution can be written as

$$\delta = 0.82\lambda \left[\frac{Z}{X_{\max}} \right], \tag{17}$$

where δ is expressed in Bubble Chamber space. The limiting resolution for $Z = 2$ m (the center of the Bubble Chamber), due to each holographic aberration independently is,

$$\delta_s \approx 24\ \mu\text{m}; \quad \delta_C \approx \left(72\sqrt[3]{\sin \alpha_o}\right)\ \mu\text{m};$$

$$\delta_A \approx (885 \sin \alpha_o)\ \mu\text{m};$$

for spherical aberration, coma and astigmatism respectively. Assuming no aberrations, $X_{\max}$ would be equal to the useful radius of the hologram, which on 70 mm film with sprocket holes is about 28 mm. This gives a diffraction limited resolution of 37 μm. Although the analysis was done only for the mismatch in wavelength, holographic resolution will also be limited by the alignment of the reconstruction beam or, in our case, the micro-positioning of the hologram.

It is seen that the resolution is mainly limited by astigmatism. Tilting the hologram with respect to the fiber can completely eliminate astigmatism. The tilt shown in fig. 1b is accomplished during micro-positioning of the hologram. Although the tilt angle is small the adjustment is easy to make because the image is so drastically improved. To understand the tilting phenomena we start with eq. (4). The parameter x_c changes during tilting so that $x_c \to x_c + \Delta x_c$. For modified inline holography $x_c = x_r = 0$, and x_c in eq. (4) becomes Δx_c. Letting $\Delta x_c / z_c = \sin \theta$ and $z_c = z_r$ for small θ, eq. (4) becomes

$$A_x = \frac{\mu \sin^2 \alpha_o}{z_r z_o} \left\{ (1-\mu^2) z_r + (\mu^2 - \mu) z_o - \frac{2 \sin \theta}{\sin \alpha_o} [(1-\mu) z_o + \mu z_r] - \frac{\sin^2 \theta}{\sin^2 \alpha_o} (z_r - z_o) \right\}. \tag{18}$$

We see then that the astigmatism will be zero for the roots of the quadratic in terms of sin θ, the tilt angle. Calculating sin θ exactly for different object angles α_o and using the usual parameters we get the following roots:

$\alpha_0 =$	5°;	10°;	15°;
$(\sin \theta)_{1,2} =$	−1.38, 0.0043;	−2.75, 0.0085;	−4.10, 0.0129;
$\theta \approx$	4.3 mrad;	8.5 mrad;	12.9 mrad.

Only the roots within the range of the sine function represent the tilt angles. The approximate solution of sin θ for small θ is

$$\sin \theta = 2 \left(\frac{(1-\mu^2) z_r + (\mu^2 - \mu) z_o}{(1-\mu) z_o + \mu z_r} \right) \sin \alpha_o. \tag{19}$$

In practice this tilt is needed about both the y-axis of the hologram and the x-axis of the hologram. Although the calculation made is about the y-axis, the method for determining the tilt about the x-axis is identical. Tilting the hologram will then eliminate the astigmatism produced by the wavelength mismatch. This, in large part, is the reason we can obtain results with a He–Ne laser which are comparable to those obtained with a dye laser tuned to the ruby wavelength [14,15].

The resolution of the fisheye lens was estimated by tracing several rays through the fisheye lens at several field positions. The maximum full field angle used in the pencil was 1.4° and corresponds to a maximum magnification on the reconstruction machine. Although the fisheye lens is a wide-angle lens, the field of view used during high magnification holographic play back is small. This is possible because the fisheye lens is concentric so that rotation of the optical axis about the center of the lens does not change the optical path for different object positions in chamber space (see fig. 1a). Table 2 shows the result of the ray trace at full field, the aberration encountered by each ray is given in terms of wave front aberration. The tolerances in table 1 are used and show that the effective half-aperture for the fisheye lens is about 10.0 mm. Using the effective aperture of 10.0 mm and object distance fo 2 m we have a resolution limit for the fisheye lens of $\Delta_F \approx 104\ \mu$m in

Table 2
Results of ray tracing

Effective half aperture [mm]	Meridional rays upper/lower	Marginal ray upper/lower	Sagittal ray
5.0	−0.003/−0.022 λ	−0.007/−0.062 λ	−0.023 λ
7.5	−0.008/−0.072 λ	−0.031/−0.218 λ	−0.099 λ
10.0	−0.023/−0.175 λ	−0.117/−0.556 λ	−0.291 λ
12.5	−0.063/−0.358 λ	−0.330/−1.181 λ	−0.686 λ
15.0	−0.173/−0.732 λ	−0.933/−2.508 λ	−1.617 λ

Table 3
Resolution in μm for 11° target

Laser wavelength	Resolution no tilt [μm]	Resolution with tilt [μm]	Measured tilt [mrad]	Predicted tilt [mrad]
He–Ne (632.8 nm)	500	177	37.9 ± 4.4	38.09
Dye laser (698 nm)	223	157	1.3 ± 4.4	2.28

air. The root squared sum (RSS) value of δ_A and δ_F is plotted in fig. 6, where δ_A is the limiting holographic resolution due to astigmatism. This provides an overall system performance estimate for reconstruction with He–Ne wavelength without tilting the hologram. When tilting the hologram $\delta_A \approx 0$, then the limiting holographic resolution becomes δ_C (the limiting holographic resolution due to coma). The RSS value of δ_C and δ_F then provides an overall performance estimate for reconstruction with He–Ne wavelength while tilting the hologram, this is also plotted in fig. 6. We have shown

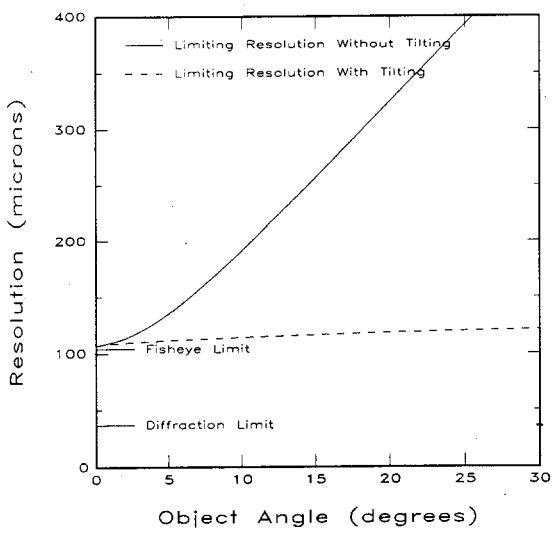

Fig. 6. The calculated resolution for reconstruction with He–Ne wavelength is shown in terms of the object angle. Solid line, $\delta = (\delta_A^2 + \delta_F^2)^{1/2}$ resolution limit without tilting. Broken line, $\delta = (\delta_C^2 + \delta_F^2)^{1/2}$ resolution limit with tilting.

what the lower limits of resolution are for different sources of aberration (omitting degrading effects during recording). The final resolution is best found by direct measurement of the system.

5.1.3. Measured resolution

Measurement of the resolution was made using a test target placed inside the empty Bubble Chamber. The test target consisted of a 1951 USAF bar target and a 5 μm wire with 100 μm glass beads glued to it. The glass beads simulate the bubbles in the cold chamber, refracting and scattering the illumination light much like bubbles. The bar target was placed one inch away from a plate of ground Plexiglas which acted as a diffuser. The entire assembly is called the test target. The test target was placed at the center of the Bubble Chamber two meters away from the holographic camera at an object angle of 11.0°. Table 3 shows the results of replaying these test holograms on the Fermilab reconstruction machine. For the warm chamber holograms the resolution is measured by identifying the smallest group of separable bar pairs on the USAF bar target, the line pair width of this group is the measured optical resolution. Two different wavelengths for reconstructing the holograms were tested. The first row shows the holograms reconstructed with the He–Ne laser with and without tilting. Row 2 shows the results of the same hologram reconstructed in row 1, but with the dye lasers. The peak emitting wavelength of the dye used is at 698 nm *. Fig. 7 shows the photographed results of

* In this calculation the wavelength of the dye laser is chosen as 698 nm because the system was tuned for peak output of the dye.

these tests. The tests show that the resolution limit as calculated has been nearly reached by the Fermilab reconstruction machine. The target reconstructed with the He–Ne laser was tilted to correct for astigmatism by the amount shown in the table. Without tilting the test target, the resolution is very poor as indicated in column one. Tilting the holograms reconstructed with the dye laser gave the best results. This may be due to the fact that the dye laser does not exactly match the ruby wavelength of the recording laser. In this case tilting by a small amount would then compensate for astigmatism but not for coma. The coma would be less for the dye laser than for the He–Ne laser since $\Delta\lambda$ is less for the dye laser, explaining the improved resolution.

In addition to these results, separate tests in a laboratory setup were made [2] to study the modified in-line scheme. The results on the resolution obtainable were comparable to the resolution results observed above. The resolution values quoted in table 3 are based on resolving separated bar pairs on the USAF bar target. These values need to be restated if one wants to know the minimum bubble size or track width observable with holography. For a single track one should expect a resolution one-half of the resolution of a bar

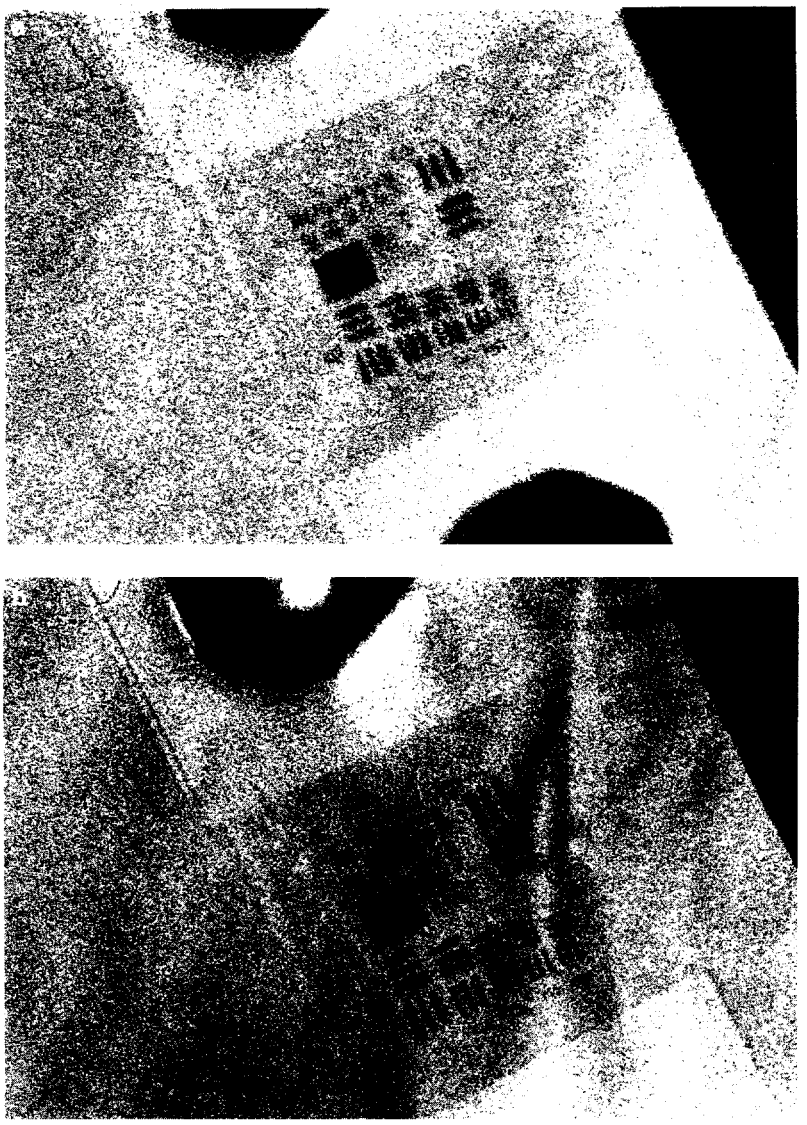

Fig. 7. Photos of reconstructed virtual holographic images taken in the warm chamber and replayed on the Fermilab Reconstruction Machine. Bar targets are at object angles of 11° with the holographic axis and at 2 m from the hologram. (a) Reconstructed with He–Ne and no tilting; (b) reconstructed with He–Ne and tilting; (c) reconstructed with dye laser and no tilting; (d) reconstructed with dye laser and tilting.

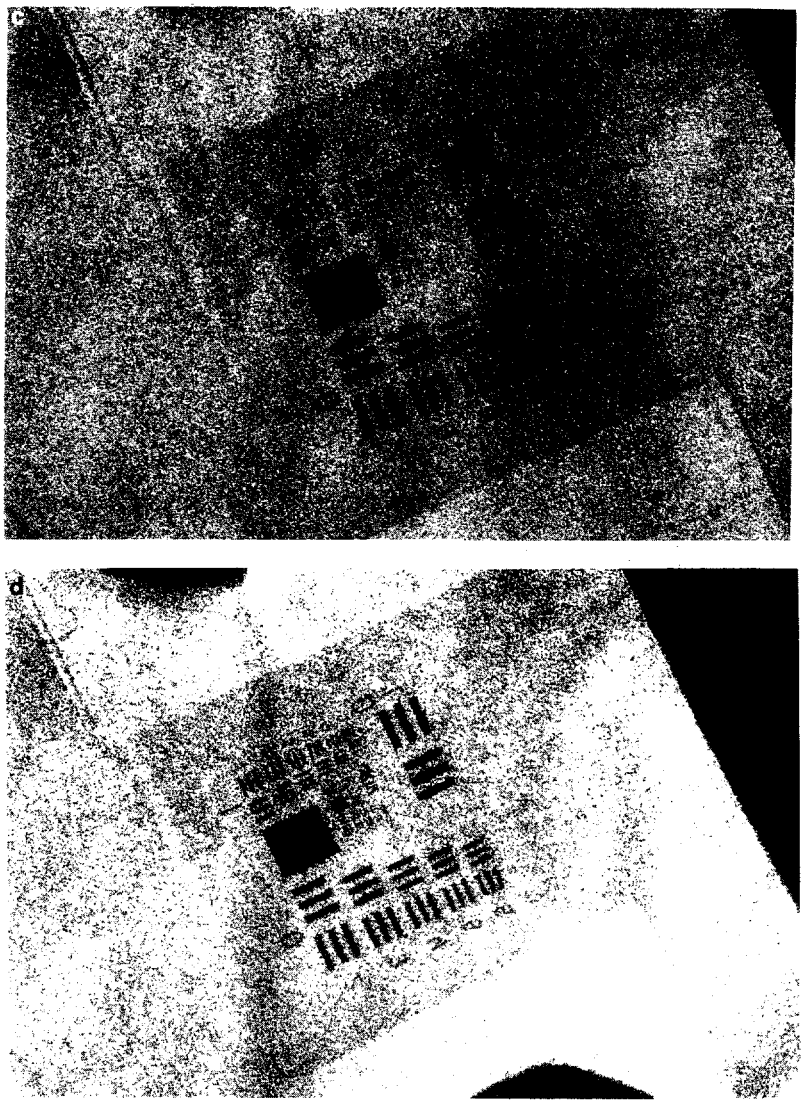

Fig. 7 (continued).

pair test target and therefore all the values in table 3 should be divided by a factor of two. For example, the best resolution for He–Ne with tilt for an 11° target is listed as 177 μm. This means that two bars of ≈ 89 μm width separated by ≈ 89 μm can be identified as two separate bars. This implies that our holographic reconstruction system can resolve bubble and track widths of the order of ≈ 100 μm. To obtain resolution limits for the cold chamber filled with a mix of Ne/H2 (62/38%) we should divide the results by the refractive index of 1.088.

5.2. Procedure for operation

The procedure for operating the holographic reconstruction machine in normal scanning mode is as follows.

(1) Conventional film is scanned, all events are labeled and the event vertex is measured and recorded in Bubble Chamber space using conventional film measurement methods. Information such as vertex position, scanner comments, number of events per frame, etc is kept in a data base. This information can then be accessed by means of a computer terminal at the holographic reconstruction facility which is located in a different building than the conventional film scanning area.

(2) At the holographic reconstruction facility the measured vertex positions for all events are then transformed (see appendix) into holographic reconstruction machine coordinates. Those events in the holographic fiducial volume are listed with their reconstruction machine coordinates and scan record.

(3) Holograms flagged in step number two are setup

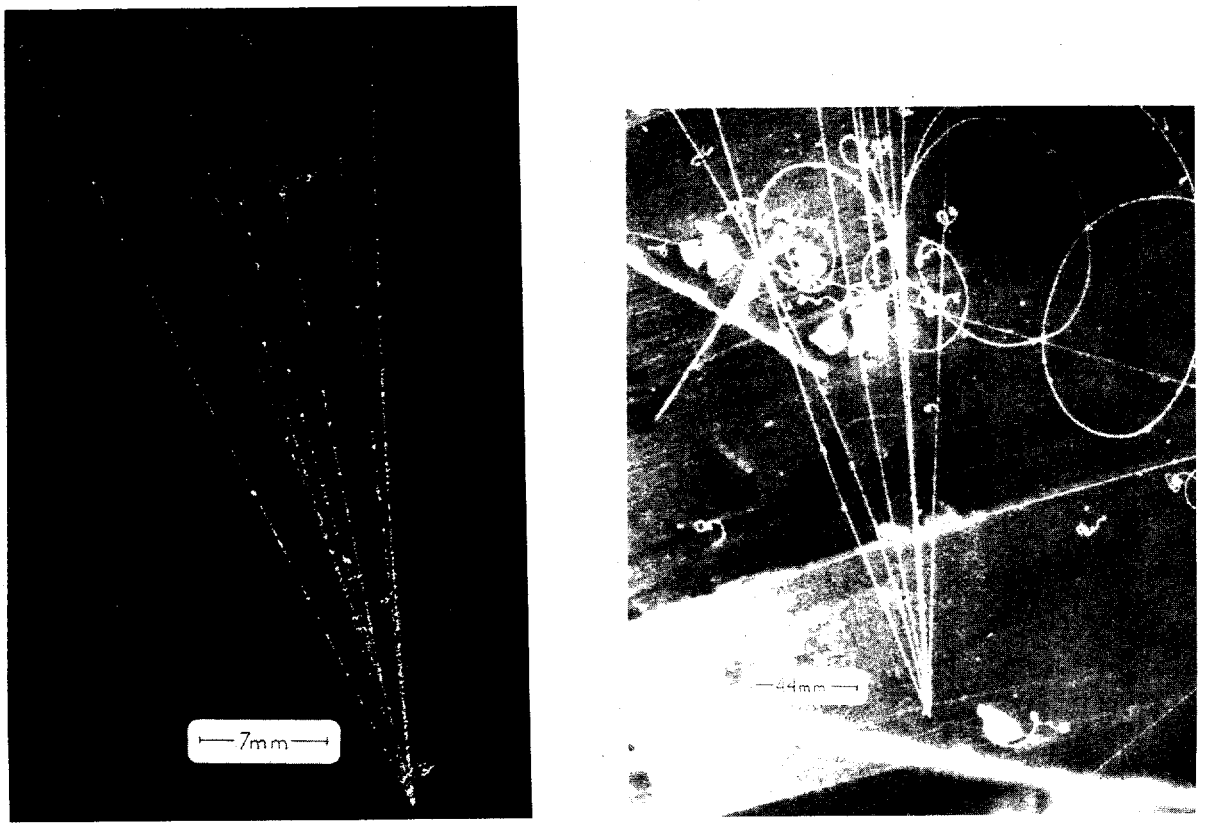

Fig. 8. Photos of the same event seen in both holographic and conventional views showing the superior resolution of the holographic view. (a) Holographic view (left); (b) conventional camera view (right). Only in (a) can one track be clearly seen to split into three tracks after some 7 mm. The scales are in Bubble Chamber space.

for inspection. The hologram is searched near the predicted event location.

(4) When the event is found, the hologram is fine tuned for best image quality and studied. If an inspection of the vertex region shows interaction or decay close to the vertex we record that there is Possible Close Activity (PCA) and make a photographic record of the reconstructed event. The PCA region is a sphere of radius 2 cm in real space.

(5) A holographic scan record is then produced containing a quality label for the hologram, information on whether the reconstruction was photographed, and the category of the event (i.e. PCA).

(6) A pool of interesting events is collected. Analysis of these events is made on the conventional film, using only the conventional measurements as the data. The holographic scan has thus served to isolate interesting events. We hope in the future to use more data directly from the hologram in the analysis process.

5.3. Results and discussion

The Fermilab holographic reconstruction machine has as its primary advantages, low cost in construction, ease of use, exceptional quality of images produced, and small overall size. The Fermilab machine is completely manual but remains convenient to operate. The micropositioning adjustments, hand cranks and camera focusing are readily available from a single location within the room making operation convenient. Although many of the controls could have been motor driven with digital readout for easier and more automated use, this was avoided because of the added complications and additional costs.

The ability to tilt the hologram has proven to be one of the most useful features of the reconstruction machine. Tilting the hologram corrects for using a different wavelength in reconstruction than was used in recording of the hologram. It also provides a method of fine tuning for film misalignment and other less understood related effects. In our case by tilting the hologram it is possible to get nearly the same resolution with a He–Ne laser as can be obtained when reconstructed with a dye laser tuned for the recording wavelength and tilting the hologram. In addition, the contrast in the photos produced when using the He–Ne laser is better, due to the improved sensitivity of the film at this wavelength. In summary, tilting the hologram allowed us to use a

He–Ne laser which is easier to employ and requires less maintenance than a dye laser, while giving comparable results.

For the holograms made in the 15 ft chamber there are two types of primary images available, virtual and real. The calculations presented are valid for both types of images. The primary difference in reconstruction of these two types of images is the reconstruction reference beam. For the real image a beam identical to the recording beam but time reversed is needed. The virtual image uses a beam identical to the recording beam. For the real image this means that the reconstruction beam must fill the hologram aperture and converge to a small reference spot. Because of the way the Bubble Chamber windows are constructed, this can be accomplished by a positive 70 mm aperture lens of focal length 32 cm placed in front of the hologram and focused through the hologram. The real image then appears on the side of the hologram opposite the lens. In the virtual image case a diverging beam originates approximately 32 cm from the hologram. This is accomplished in our case by the optical fiber described earlier. For best results a reconstruction beam should be spatially filtered. In our virtual image case this is automatically done by the optical fiber. For comparable reference beams the resulting real and virtual images should be equal in quality. In practice it is easier to produce a spatially filtered diverging reference beam with a small spot size and for this reason the virtual image was chosen for the Fermilab system. Real image machines with fisheye compensating optics have been built at other facilities [16,17].

We have built a holographic virtual image reconstruction machine for the reconstruction of holograms taken in the Fermilab 15 ft Bubble Chamber. We have discussed the major components of the holographic reconstruction machine and the construction details which were specific and important to our design. The resolution limit using a He–Ne laser has been calculated and measured and meets our requirements for resolution. The resolution of the system was improved by using a liquid film gate. The usefulness of this system is enhanced by the flexibility of using a fiber optic reconstruction reference beam. A procedure for locating 15 ft Bubble Chamber data on the holograms has been outlined.

Reconstruction systems for holograms of this type could be used for various high resolution holographic nondestructive testing schemes (HNDT), e.g. for industrial products or components and in particular the inspection of nuclear fuel elements and other nuclear reactor components [18].

Acknowledgements

We wish to acknowledge the assistance of the technicians and machinists under the direction of Dr. Wes Smart and Jim Kilmer in the development of this system. The help of Dr. H. Akbari in the initial tests is acknowledged. Dan Snee helped construct portions of the apparatus. Finally the assistance of our colleagues on E-632 is greatly appreciated. **The support provided IIT by the National Science Foundation is herewith acknowledged.**

Appendix

Holographic transformations

To transform from Bubble Chamber space to holographic reconstruction space a series of transformations were used. The first transformation transforms coordinates from real Bubble Chamber space to virtual fisheye lens space. The other transformation used is to correct for image shift due to incorrect reconstruction wavelength and reference beam misalignment.

Since the holographic camera has a fisheye lens in front of it (fig. 1a), the virtual image space of the hologram is coincident with the virtual image of the fisheye lens. This fisheye lens acts approximately like a negative lens of focal length −32 cm. To first approximation the image distance can easily be found using the focal length of the lens. A more precise method is to trace paraxial rays through the fisheye lens for all object distances. This will give the position of the image on axis. Since the fisheye lens is concentric the optical axis is optically invariant upon rotation about the center of the spherical lens (fig. 1a). Because the optical axis is invariant upon rotation the image distance of an object off-axis can be found by tracing paraxial rays from an auxiliary axis pointing at the off-axis object. This simplifies image distance calculation, since no oblique rays need be traced. Also the angles which define the auxiliary axes are equivalent in both object and image space. The Fermilab Reconstruction Machine defines the auxiliary axes by dip and azimuth angles whose adjustments are directly made on the moving stage.

The following describes the transformation used to correct for reconstruction wavelength and reference beam misalignment. Starting with Meier's [19] equations for the position of the Gaussian (or first-order) image point located at (x_i, y_i, z_i), given the object point (x_0, y_0, z_0) we have

$$x_i = \frac{m^2 x_c z_o z_r + \mu m x_o z_c z_r - \mu m x_r z_c z_o}{m^2 z_o z_r + \mu z_c z_r - \mu z_c z_o};$$

$$y_i = \frac{m^2 y_c z_o z_r + \mu m y_o z_c z_r - \mu m y_r z_c z_o}{m^2 z_o z_r + \mu z_c z_r - \mu z_c z_o};$$

$$z_i = \frac{m^2 z_c z_o z_r}{m^2 z_o z_r + \mu z_c z_r - \mu z_c z_o};$$

where m is the magnification of the interference pattern recorded on the film. For example, if x' and y' were the coordinates in the hologram during recording and x and y the coordinates after an enlargement or reduction, then $x = mx'$. The wavelength ratio of reconstruction to recording light is $\mu = \lambda_c/\lambda_r$r. The terms (x_r, y_r, z_r) and (x_c, y_c, z_c) are the location of the recording and reconstruction reference beams respectively.

For modified in-line holography the reference beam is on axis so that $x_r = y_r = 0$. The extent to which $x_c = x_r$ and $y_c = y_r$, depends on micro-positioning the hologram. This does not affect image location since the image shift during micro-positioning is an order of magnitude less than the field of view seen on the video monitor. Since the hologram has not been scaled up or down unit magnification $m = 1$ is used. Taking into account the preceding we get

$$x_i = \frac{\mu x_o z_c z_r}{z_o z_r + \mu z_c z_r - \mu z_c z_o},$$

$$y_i = \frac{\mu y_o z_c z_r}{z_o z_r + \mu z_c z_r - \mu z_c z_o},$$

$$z_i = \frac{z_c z_o z_r}{z_o z_r + \mu z_c z_r - \mu z_c z_o}.$$

Of course the reverse can also be done knowing the position of the virtual image point, the real object point can be determined by solving for x_0, y_0, z_0. This was done during the run in the monitoring process for holographic film test strips. Since one could determine the coordinate of a particular event in the Bubble Chamber it was then possible to map the holographic sensitive region quickly and get immediate feedback on laser performance. Measuring the position of vertices from the hologram had an error of ± 2 cm in x and y, and ± 5 cm in z. This was of sufficient accuracy for monitoring the holographic volume at run time. The errors in x and y are due to the lack of systematic positioning of the holograms and to backlash of the turntables which in turn made repeatable readings difficult. The error in the z-coordinate is primarily due to the best focus method used in defining the image plane. Since the best focus has a range of values which are subjective, the method is limited by the depth of focus. Absolute measurements of vertex coordinates of events in Bubble Chamber space can be made with greater precision if high precision stages are purchased. This has not been necessary in our case.

References

†Permanent Address: Illinois Institute of Techology, Chicago, IL

‡Permanent Address: Northwestern University, Evanston, IL

[1] H.I. Bjelkhagen et al., Nucl. Instr. and Meth. 227 (1984) 437.
[2] H.I. Bjelkhagen, CERN 85-10 (1985) p. 7.
[3] G. Harigel et al., Appl. Optics 25 (1986) 4102.
[4] J.K. Hawkins and W.A. Williams, Proc. SPIE 927 (1988) 180.
[5] D.A. Delwiche, J.D. Clifford and W.R. Weller, J. Sci. Motion Picture Tech. 67 (1958) 678.
[6] H.M. Smith, Principles of Holography (Wiley, New York, 1975) p. 143.
[7] R.W. Meier, J. Opt. Soc. Am. 57 (1967) 895.
[8] B. Champagne and N.G. Massey, Appl. Optics 8 (1969) 1879.
[9] D.H.R. Vilkomerson and D. Bostwick, Appl. Optics 6 (1967) 1270.
[10] Ref. [6], p. 173.
[11] Ref. [6], p. 174.
[12] M. Born and E. Wolf, Principles of Optics (Pergamon, London, 1983) p. 472.
[13] Ref. [12], p. 424.
[14] M. Austin, J. Phys. D: Appl. Phys. 17 (1984) 1953.
[15] I. Banyasz, Appl. Optics 27 (1988) 1293.
[16] P. Nailor, CERN Report 85-10 (1985) p. 85.
[17] M.W. Peters and R.J. Cence, CERN Report 85-10 (1985) p. 95.
[18] B.A. Tozer et al., Opt. Eng. 24 (1985) 746.
[19] R.W. Meier, J. Opt. Soc. Am. 55 (1965) 987.